Supporting Information

Study of the Doping Effect on Imperfect Morphology at Photovoltaic Heterojunction in Bilayer Organic Solar Cells

Zhenyu Chen, [a] Hong Zheng[*, b] Wei Ma, [a] Han Yan[*a, c]

Table of content

Experimental section

Materials: PBDB-T and ITIC were purchased from Solarmer Materials Inc. F6TCNNQ was purchased from Sigma-Aldrich. All chemicals were used as received without further purification.

Instrumentation: The GIWAXS measurements of the control and doped films were performed at beamline 7.3.3 at the Advanced Light Source. [1] Samples were prepared on Si substrates using identical blend solutions as those used in devices. The 10 keV X-ray beam was incident at a grazing angle of 0.11°-0.15°. The scattered x-ray was detected using a Dectris Pilatus 2M photon counting detector.

The *J–V* curves were performed in the N2-filled glovebox under AM 1.5G (100 mW cm^{-2}) using an AAA solar simulator (SS-F5-3A, Enli Technology Co., Ltd.) calibrated with a standard photovoltaic cell equipped with KG5 filter. The *EQE* curves were measured by Solar Cell Spectral Response Measurement System QE-R3018 (Enli Technology Co., Ltd.) with calibrated light intensity by a standard Si photovoltaic cell. The absorbance spectra were obtained on a Shimadzu UV-3600 Plus Spectrophotometer.

EL measurement uses the direct-current meter (PWS2326, Tectronix) to provide bias voltage to the device, then the luminous signals are collected by fluorescence spectrometer (KYMERA-328I-B2, Andor technology LTD). The EQE_{EL} measurement system is consisted of a Keithley 2400 digital source meter, Keithley 6482 picoammeters and a standard Si detector (S1337-1010Br). For the sensitive *EQE* (*sEQE*) measurement, the light from halogen light source (LSH-75, Newport) becomes monochromatic light by using a monochromator (CS260-RG-3-MC-A, Newport), and is focused on the device to generate electrical signals. Then the signals are

amplified by the front-end current amplifier (SR570, Stanford) and finally collected by the phase-locked amplifier (Newport). The *EQE* spectrum was obtained by using the corrected Si standard detector (S1337-1010Br).

PL spectrum was recorded by FLS980 spectrometer (Edinburgh Instruments, EI) with different excitation wavelength. Temperature-dependent measurement was kept from the temperature range of 78-298 K.

Device Fabrication: The PHJ devices were fabricated with a configuration of ITO/ZnO/ITIC/PBDB-T/MoO_X/Al. The ITO substrates were cleaned by sequential sonication and UVO treatment. The electron-transporting layer of ZnO was deposited by spin-coating a ZnO precursor solution (dissolving zinc acetate in 2-methoxyethanol with ethanolamine) at 4500 rpm for 30s, followed by thermal annealing at 200 ℃ for 30 min. ITIC (10mg/mL) was spin-coated on the ZnO layer with thickness of ~20 nm. F6TCNNQ was dissolved by ethanol with optimized concentration and process with the spin speed at 6000 rpm for 25s. The PEDOT:PSS was spin-coated on the cleaned glass substrate as a sacrificed layer at 1500 rpm for 30s, followed by thermal annealing at 150 ℃ for 2 min. As a transfer-film, PBDB-T (10 mg/mL PBDB-T(CB) and 8 mg/ml for PBDB-T(TL)) was spin-coated on the PEDOT:PSS, keeping the PBDB-T film thickness at ~30 nm. For the doped sample, the F6TCNNQ ethanol solution was coated on PBDB-T layer. The transfer-layer (with a structure of glass/PEDOT:PSS/PBDB-T) was immersed in deionized water. After the dissolution of PEDOT:PSS, the PBDB-T layer floated on water. Then we used the ITIC coated ZnO/ITO substrate to stick on top of the PBDB-T layer, simultaneously forming the bilayer heterojunction. Finally, 10 nm MoO_3/100 nm Al were deposited as the electrode at a vacuum level of < 1×10^{-5} Pa.

Calculating the energy loss: The total energy loss is composed of three parts as is shown by

$$q\Delta V_{loss} = E_g^{PV} - qV_{OC} \quad \text{(S1)}$$

$$= \left(E_g^{PV} - E_{CT}\right) + \left(E_{CT} - qV_{OC,\ rad}\right) + \left(qV_{OC,\ rad} - qV_{OC}\right)$$

$$= \left(E_g^{PV} - E_{CT}\right) + q_\Delta V_r + q\Delta V_{nr}$$

where ΔV_{loss} is the total voltage loss, E_g^{PV} is the photovoltaic bandgap energy, E_{CT} is the CT state energy, $V_{OC,\ rad}$ is the voltage with only radiative recombination at open circuit condition, ΔV_r is the radiative recombination voltage loss owing to absorption edge broadening effects, ΔV_{nr} is the nonradiative recombination voltage loss due to the EL radiative efficiency. $q\Delta V_{nr}$ is calculated by

$$q\Delta V_{loss} = -k_B T EQE_{EL} \quad \text{(S2)}$$

The E_g^{PV} is determined by [12]

$$E_g^{PV} = \frac{\int_a^b EP(E)dE}{\int_a^b P(E)dE} \quad \text{(S3)}$$

where $P(E) = dEQE_{PV}/dE$, EQE_{PV} is determined by the *sEQE* measurement, E is the photon energy, a and b are selected where $P(a) = P(b) = 0.5\max[P(E)]$. The CT state is extracted by simultaneously fitting the black-body spectrum (φbb) calibrated absorption spectrum (Equation (S4)) and the measured emission spectrum (Equation (S5)):

$$\sigma(E)dE = \frac{f}{\sqrt{4\pi\lambda k_B T}} exp\left(\frac{-\left(E_{CT} + \lambda - E\right)^2}{4\lambda k_B T}\right)$$

(S4)

$$\frac{I(E)}{E} = \frac{f}{\sqrt{4\pi\lambda k_B T}} exp\left(\frac{-\left(E_{CT} - \lambda - E\right)^2}{4\lambda k_B T}\right)$$

(S5)

where f is the absorption oscillator strength and λ is the reorganization energy.

Calculating the polar angle: A pole figure is a representation of the orientation distribution of crystallographic planes in a sample, which illustrates the texture of a material. ω is defined as the angle between the scattering vector and the substrate normal. The scattering intensity near ω = 0° and 90° is associated with face-on (Axy) and edge-on (Az) orientations relative to the substrate, respectively. The value of Axy/Az is a measurement of face-on contribution, defined as the ratio between the integrated area (Axy) where 0° < ω < 45° and the area (Az) where 45° < ω < 90° according to the reference. [2]

Calculating the number of lamellar or pi-pi stacking layers: The calculation method First, we obtained the location of lamellar or π-π peak from the GIWAXS patterns, and the coherence length (CL) was calculated from its full width at half maximum (FWHM) as below

$$CL = \frac{2\pi \times 0.9}{FWHM}$$

The distance between two neighboring layers along the lamellar or π-π direction was calculated by the corresponding scattering vector of the two peaks

$$d = \frac{2\pi}{q}$$

Therefore, we calculate the number of lamellar or pi-pi stacking layers by

$$n = \frac{CL}{d}$$

This method has been reported by Ye et al. before.[3]

Computational details： The poly PBDB-T material was simulated with a fragment strucutre including three monomer units ended with H was constructed, in which totally 470 atoms are included. In the film structure composed of a PBTB-T fragment and a p-dopant (F6TCNNQ) molecule, different orientations of F6TCNNQ induces two types of conformations, the face-to-face (f-f) and edge-to-face (e-f) structures. In the f-f structure, the F6TCNNQ molecule faces to the lamellar of PBDB-T. The e-f structure can be further defined as two kinds of conformers, in which the F6TCNNQ molecule faces to two sides of the lamellar of PBDB-T. In all these structures, the p-dopant is located around the center unit of the PBDB-T fragment. The interaction between PBDB-T and F6TCNNQ is dominated by van der Waals force. Therefore, the DFT method with the B97XD functional was utilized in the geometrical optimizations because it contains semi-empirical dispersion corrections.[4] In geometrical optimizations, the LanL2DZ basis set with the Los Alamos effective core potentials (ECPs) was used for the S atoms, [5] while other atoms were calculated with the usual splitting valence basis set 6-31G(d). [6-9] Further analyses of frontier molecular orbital, electrostatic potential, and quadrupole component were based upon single point calculations for the individual PBDB-T/F6TCNNQ structures and f-f/e-f conformers. In the single point calculations, a larger basis set 6-311G(d,p) [9] was used for the F6TCNNQ molecular. For the first-row elements in the PBDB-T fragment, to reduce the computational cost, only the center monomer unit was calculated with the 6-311G(d,p) basis set, whereas other parts were calculated with the 6-31G(d) basis set. The S atom was still calculated with the LanL2DZ basis set. All the DFT calculations were conducted with the Gaussian16 package. [10] In addition, the analyses of electrostatic potential were carried out with the Multiwfn_3.7 program.[11]

Figures

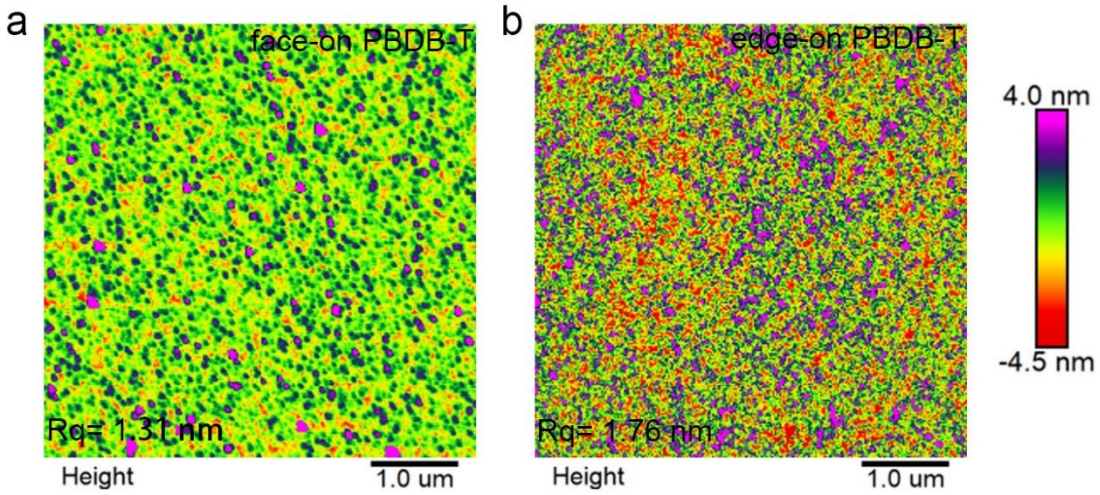

Fig. S1 AFM images of PBDB-T films via different solvent deposition: (a) f-PBDB-T with CB process and (b) e-PBDB-T with TL process.

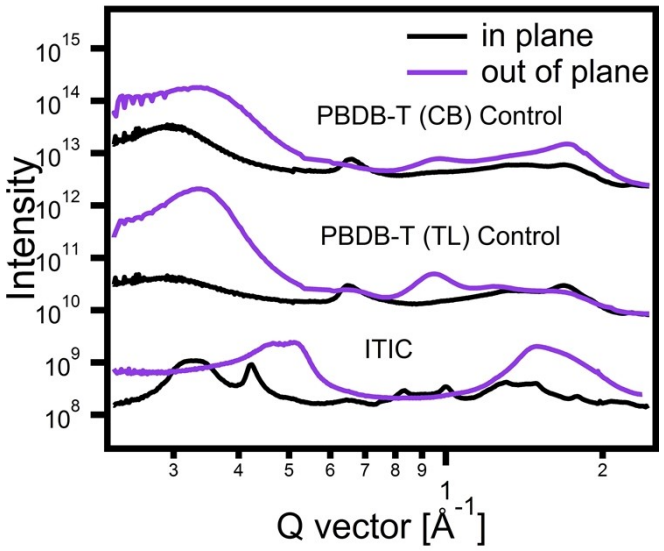

Fig. S2 In plane and out of plane line cuts of PBDB-T (CB), PBDB-T (TL) and ITIC films.

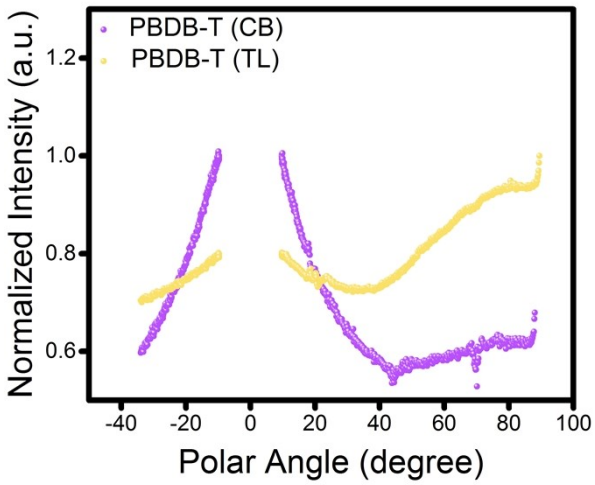

Fig. S3 Pole figures of (010) diffraction peaks for PBDB-T (CB) and PBDB-T (TL) films in out of plane direction.

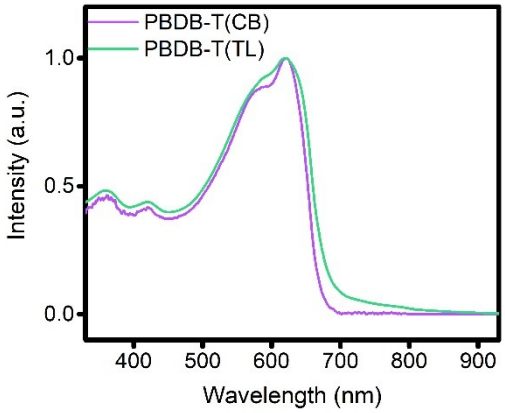

Fig. 4 The solution absorption spectra of PBDB-T in CB and TL.

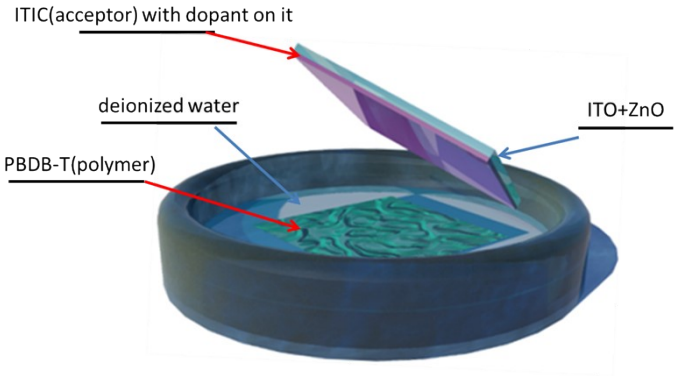

Fig. S5 Cartoon of the PHJ device fabrication process.

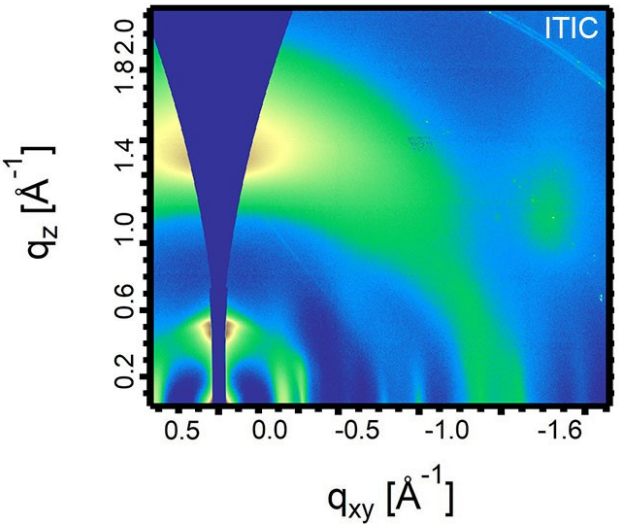

Fig. S6 Two-dimensional GIWAXS pattern of ITIC film.

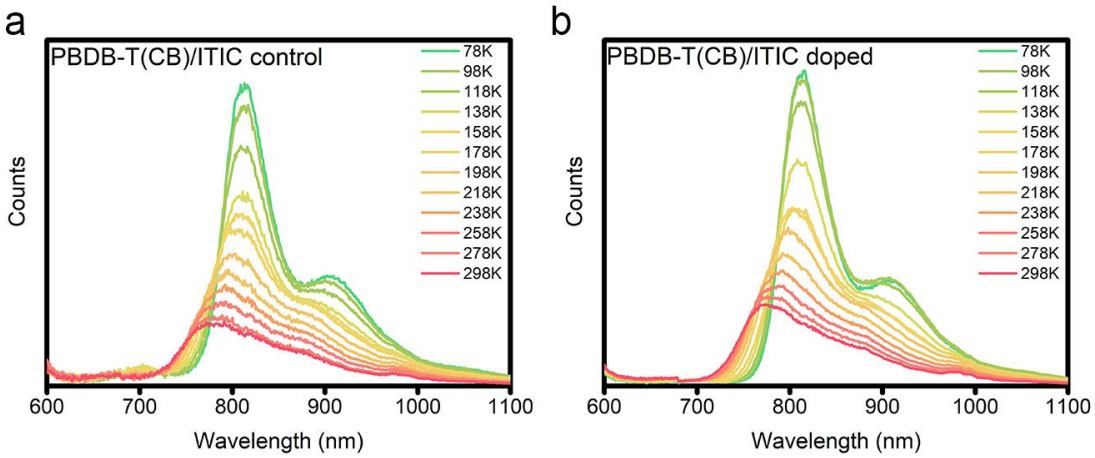

Fig. S7 Temperature-dependent photoluminescence (PL) spectra for (a) PBDB-T(CB)/ITIC PHJ control films and (b) PBDB-T(CB)/ITIC PHJ doped films. The films excited at 580 nm, and measured with the range from 600 to 1100 nm. The temperature is selected from 78 K to 298 K.

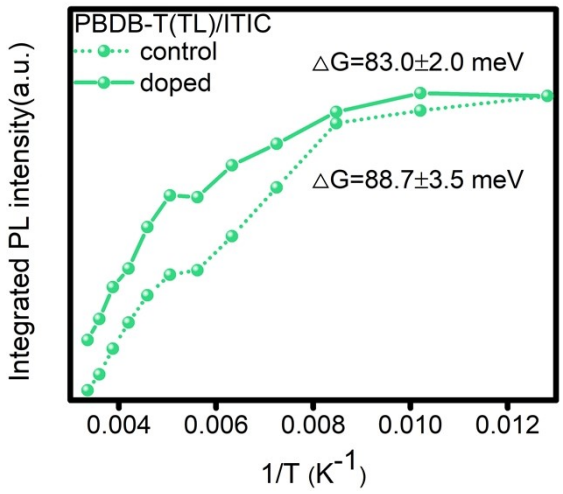

Fig. S8 Evolution of PL intensity as a function of temperature from 78 to 298 K for the ITIC film in PBDB-T(TL)/ITIC based devices.

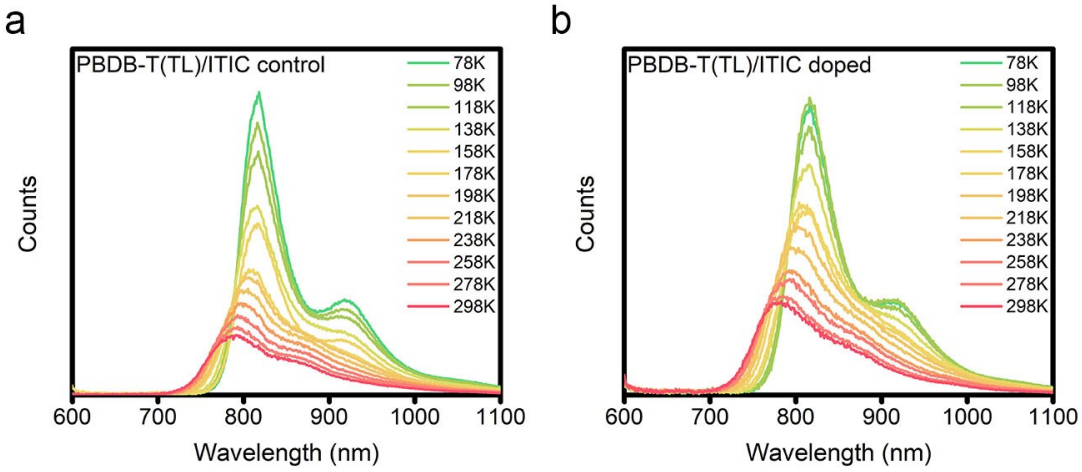

Fig. S9 Temperature-dependent photoluminescence (PL) spectra for Figure S6. (a) PBDB-T(TL)/ITIC PHJ control films and (b) PBDB-T(TL)/ITIC PHJ doped films. The films excited at 580 nm, and measured with the range from 600 to 1100 nm. The temperature is selected from 78 K to 298 K.

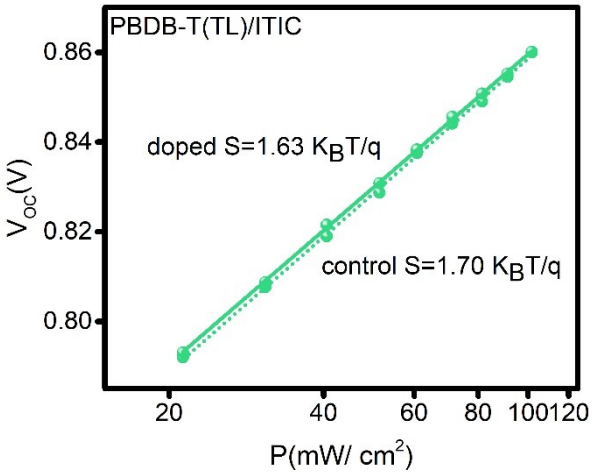

Fig. S10 Open circuit voltage (V_{OC}) of PBDB-T(TL)/ITIC with and without F6TCNNQ doped as a function of light intensity (P_{light}).

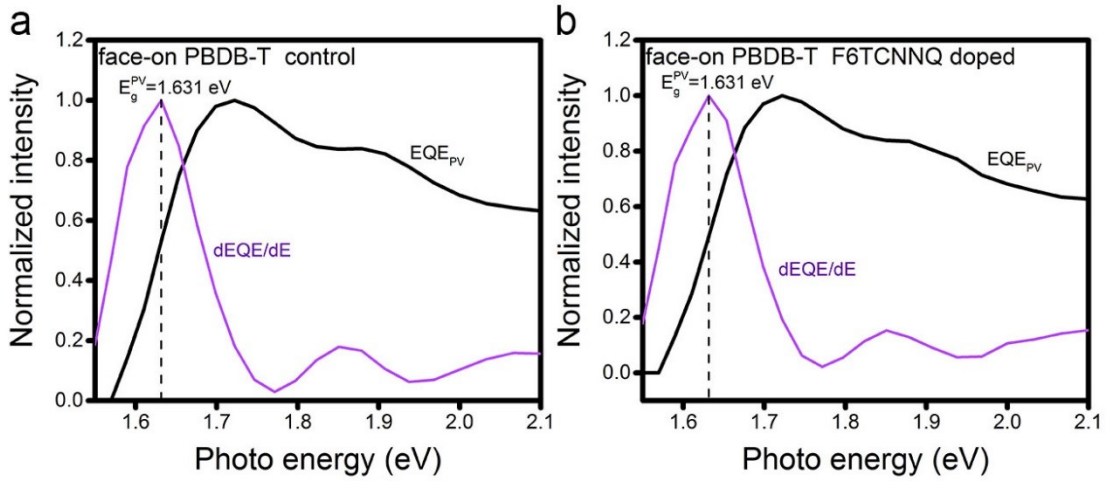

Fig. S11 The determination of device band-gap energy (E_g^{PV}) from EQE spectra: (a) f-f control device and (b) f-f doped device.

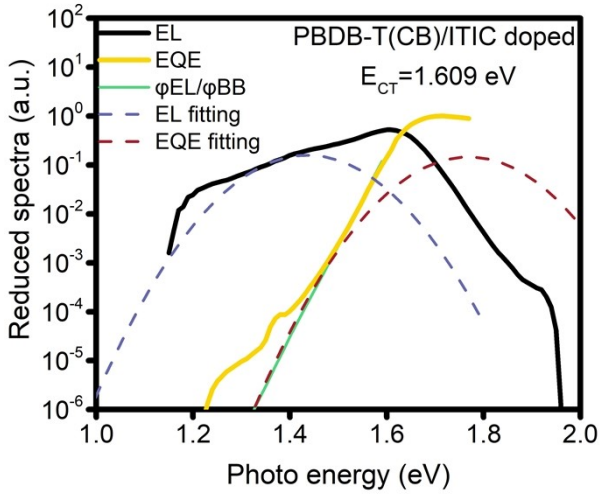

Fig. 12 Reduced sEQE and EL spectrum of a PBDB-T(CB)/ITIC doped PHJ device. The dash lines are fits of sEQE and EL for obtaining the E_{CT}.

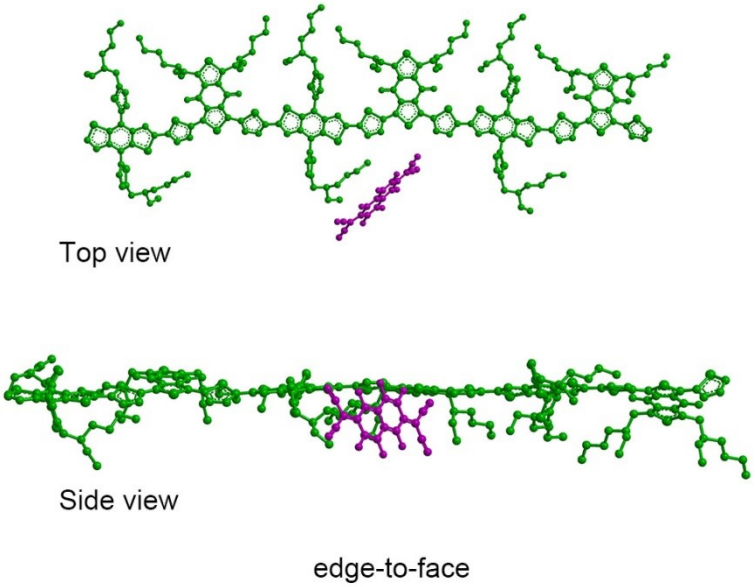

Fig. S13 Complex conformation of another e-f structure film (e-f B model).

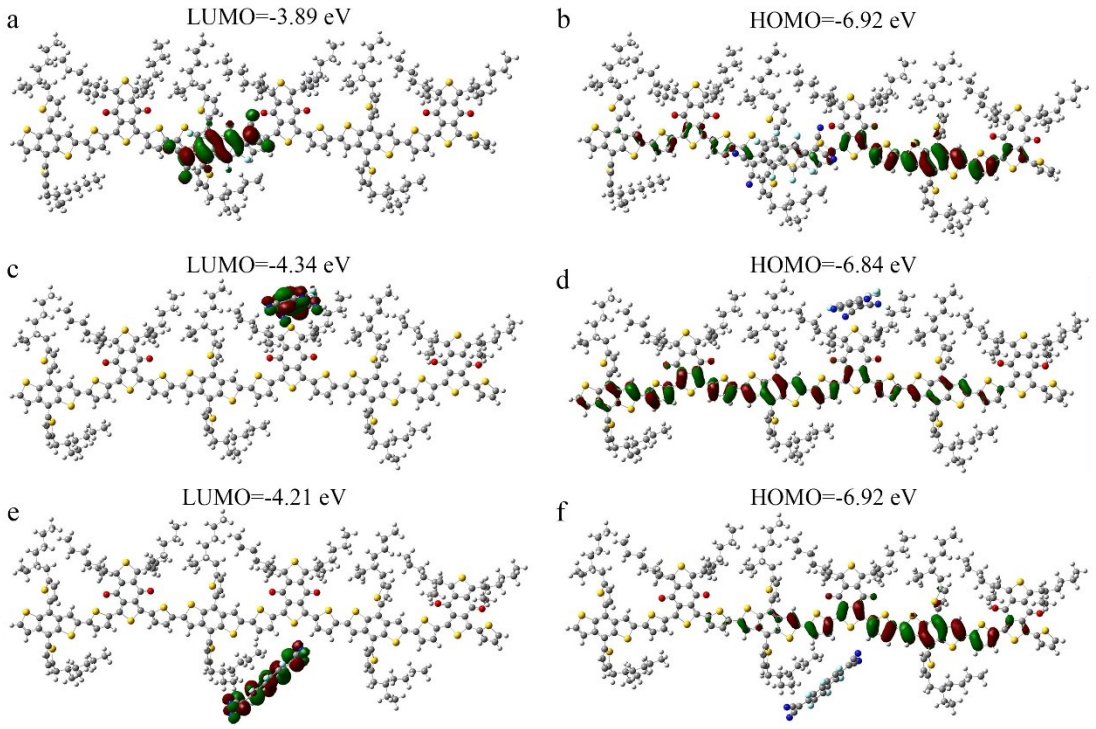

Fig. S14 The frontier molecular orbitals [lowest unoccupied (LUMO) and highest occupied molecular orbital (HOMO)] obtained by DFT calculations for complex structure molecules of (a, b) F6TCNNQ/face-on PBDB-T, (c, d) F6TCNNQ/edge-on PBDB-T A model and (e, f) F6TCNNQ/edge-on PBDB-T B model.

References

1 A. Hexemer, W. Bras, J. Glossinger, E. Schaible, E. Gann, R. Kirian, A. MacDowell, M. Church, B. Rude and H. Padmore, *J. Phys. Conf. Ser*., 2010, **247**, 012007.
2 L. Ye, Y. Xiong, Z. Chen, Q. Zhang, Z. Fei, R. Henry, M. Heeney, B. T. O'Connor, W. You and H. Ade, *Adv.Mater.*, 2019, **31**, 1808153
3 L. Ye, Y. Xiong, Q. Zhang, S. Li, C. Wang, Z. Jiang, J. Hou, W. You and H. Ade, *Adv. Mater*., 2018, **30**, 1705485.
4 J.-D. Chai and M. Head-Gordon, *Phys. Chem. Chem. Phys*., 2008, **10**, 6615–6620.
5 P. J. Hay and W. R. Wadt, *J. Chem. Phys.,* 1985, **82**, 284–298.
6 W. J. Hehre, R. Ditchfield and J. Pople, *J. Chem. Phys.,* 1972, **56**, 2257–2261.
7 R. Ditchfield, W. J. Hehre and J. A. Pople, *J. Chem. Phys.,* 1971, **54**, 724–728.
8 P. C. Hariharan and J. A. Pople, *Theoret. chim. Acta,* 1973, **28**, 213–222.
9 R. Krishnan, J. S. Binkley, R. Seeger and J. A. Pople, *J. Chem. Phys*., 1980, **72**, 650–654.
10 Gaussian.; A. Revision, M. J. Frisch, G. W. Trucks, H. B. Schlegel, G. E. Scuseria, M. A. Robb, J. R. Cheeseman, G. Scalmani, V. Barone, G. A. Petersson, H. Nakatsuji, X. Li, M. Caricato, A. V. Marenich, J. Bloino, B. G. Janesko, R. Gomperts, B. Mennucci, H. P. Hratchian, J. V. Ortiz, A. F. Izmaylov, J. L. Sonnenberg, D. Williams-Young, F. Ding, F. Lipparini, F. Egidi, J. Goings, B. Peng, A. Petrone, T. Henderson, D. Ranasinghe, V. G. Zakrzewski, J. Gao, N. Rega, G. Zheng, W. Liang, M. Hada, M. Ehara, K. Toyota, R. Fukuda, J. Hasegawa, M. Ishida, T. Nakajima, Y. Honda, O. Kitao, H. Nakai, T. Vreven, K. Throssell, J. A. Montgomery, Jr. J. E. Peralta, F. Ogliaro, M. J. Bearpark, J. J. Heyd, E. N. Brothers, K. N. Kudin, V. N. Staroverov, T. A. Keith, R. Kobayashi, J. Normand, K. Raghavachari, A. P. Rendell, J. C. Burant, S. S. Iyengar, J. Tomasi, M. Cossi, J. M. Millam, M. Klene, C. Adamo, R. Cammi, J. W. Ochterski, R. L. Martin, K. Morokuma, O. Farkas, J. B. Foresman, and D. J. Fox, Gaussian, Inc., Wallingford CT, 2016.
11 T. Lu and F. J. Chen, *Comput. Chem*., 2012, **33**, 580–592.